JOURNAL OF GUIDANCE, CONTROL, AND DYNAMICS
Vol. 19, No. 1, January–February 1996

Strategic Intercept Midcourse Guidance Using Modified Zero Effort Miss Steering

Brett Newman*
Old Dominion University, Norfolk, Virginia 23529

The suitability of modified proportional navigation, or an equivalent zero effort miss formulation, for strategic intercepts during midcourse guidance, followed by a ballistic coast to the endgame, is addressed. The problem is formulated in terms of relative motion in a general, three-dimensional framework. The proposed guidance law commands thrust 1) along the line of sight unit direction and 2) along the zero effort miss component that is perpendicular to the line of sight. The latter term is scaled with a guidance gain. If the guidance law is to be suitable for longer range targeting applications with significant ballistic coasting after burnout, zero effort miss computations must account for the different gravitational accelerations experienced by each vehicle. Approximations for the true differential gravity effect, which relieve the burden for direct numerical propagation of the governing equations, are considered. Approximations considered are constant, linear, quadratic, and linearized inverse square models. Theoretical results are applied to a numerical engagement scenario, and the resulting performance is evaluated in terms of the miss distances determined from nonlinear simulation.

Introduction

IN the overall strategic defense systems being proposed today, an essential element is the capability to engage incoming re-entry vehicles or adversarial satellites and to destroy by collision.[1] With a ground-based system, the interceptor trajectory consists of three actively guided stages: boost to accelerate beyond the atmosphere, midcourse to steer along a collision trajectory with the target, and endgame to correct for any remaining position and velocity errors. Guidance laws during the midcourse and endgame stages are key to a successful intercept.

Proportional navigation is the tried and tested guidance law for close-in, air-to-air and air defense systems.[2–7] Because of the success the technique has seen, proportional navigation will undoubtedly play a role in strategic intercepts, especially during the endgame. However, this paper is concerned with midcourse guidance strategies that are followed by a long ballistic coast to intercept. In strategic defense applications during midcourse burn, targeting distances can approach thousands of kilometers, with a significant component normal to the Earth surface. This geometry can lead to significant gravitational acceleration between the two vehicles, normal to the line of sight. If conventional proportional navigation is used for midcourse guidance, then during coast after burnout, the acceleration difference causes the relative position and velocity to drift, resulting in a miss dependent upon the coast time to intercept. Therefore, a modified guidance law correcting for gravitational differences will, at the least, be necessary.[8–11] Modifications of this sort and related to augmented proportional navigation, which corrects for accelerations from a maneuvering target.[6,7]

Theoretically, Lambert-based guidance laws[7,12,13] overcome this difficulty by accounting for the variable acceleration influencing the interceptor as it flies to a predetermined target solution. For practical implementation, however, proportional navigation based schemes hold a key advantage.[14] Lambert-based guidance laws are very sensitive to predicted vs actual motor performance. On the other hand, proportional navigation based guidance laws are robust to these uncertainties. Proportional navigation will not replace Lambert type guidance for extremely long targeting applications. However, it remains to be seen what role proportional navigation can play in intermediate range targeting applications, such as during the midcourse phase.

In this paper, the use of modified zero effort miss steering for midcourse guidance, followed by a ballistic coast, is considered. Corrections to the miss computation and thrusting direction are considered to account for the postburnout accelerations, without introducing heavy in-flight computational burdens. One technique, which appears particularly promising, joins conventional intercept guidance with space rendezvous gravity models. This is a unique result not appearing in the guidance literature. The goal of the research is to assess the feasibility of using modified conventional based intercept guidance schemes in unconventional applications (i.e., orbital motions and increased targeting distances with ballistic coasting after burnout).

Zero Effort Miss Formulation

The relevant geometry of the strategic intercept is given in Fig. 1; $\boldsymbol{R}_I$ and $\boldsymbol{R}_T$ represent the position vectors of the interceptor and target vehicles, respectively, whereas $\boldsymbol{V}_I$ and $\boldsymbol{V}_T$ correspond to their inertial velocities. The XYZ reference frame is inertial with origin located at the Earth's center. Here, the Earth's gravitational acceleration is modeled as an ideal inverse square field. In addition to illustrating the inertial trajectories, Fig. 1 also shows the relative trajectory with $\boldsymbol{R} = \boldsymbol{R}_T - \boldsymbol{R}_I$ and $\boldsymbol{V} = \boldsymbol{V}_T - \boldsymbol{V}_I$ denoting the position and inertial velocity of the target with respect to the interceptor. The relative trajectory plays a key role in zero effort miss guidance, as seen later.

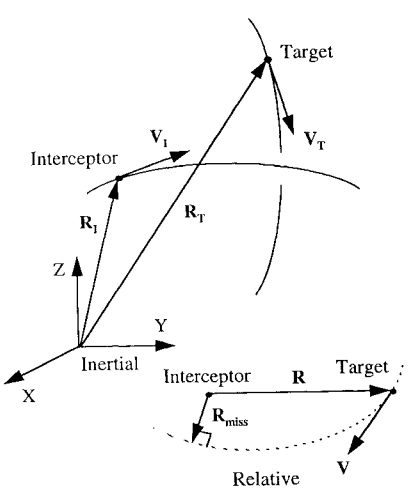

Fig. 1 Strategic intercept geometry.

Presented as Paper 93-3890 at the AIAA Guidance, Navigation, and Control Conference, Monterey, CA, Aug. 9–11, 1993; received Aug. 25, 1993; revision received Jan. 10, 1995; accepted for publication June 5, 1995.

*Assistant Professor, Department of Aerospace Engineering. Senior Member AIAA.

The governing equations of motion for both vehicles are[12]

$$\dot{V}_T = -\left(\mu/R_T^2\right)\varepsilon_T, \qquad \dot{V}_I = -\left(\mu/R_I^2\right)\varepsilon_I + (1/m)\boldsymbol{T} \quad (1)$$

where $\varepsilon_T = \boldsymbol{R}_T/R_T$ and $\varepsilon_I = \boldsymbol{R}_I/R_I$ denote unit vectors, μ is the Earth gravitational constant, m is the interceptor mass, T is the interceptor thrust vector, and "$\cdot$" denotes the time derivative with respect to the inertial frame. Relative motion between the vehicles is governed by the following differential equation

$$\dot{\boldsymbol{V}} = -\mu\left[\left(1/R_T^2\right)\varepsilon_T - \left(1/R_I^2\right)\varepsilon_I\right] - (1/m)\boldsymbol{T} \quad (2)$$

Observe the difficulty in solving Eq. (2), in closed form, for $\boldsymbol{R}$ and $\boldsymbol{V}$ due to the nonlinear gravitational term, which defies explicit expression solely as a function of the line of sight.

The zero effort miss, denoted as $\boldsymbol{R}_{\text{miss}}$, is defined here as the minimum $\boldsymbol{R}$ that results when the interceptor thrust in nulled [$\boldsymbol{T} = \boldsymbol{0}$ in Eq. (2)] and both vehicles coast under the acceleration of gravity. Kinematically, $\boldsymbol{R}_{\text{miss}}$ is the specific $\boldsymbol{R}$ that becomes perpendicular to $\boldsymbol{V}$ or satisfies

$$\boldsymbol{V} \cdot \boldsymbol{R} = 0 \quad (3)$$

An exact calculation for $\boldsymbol{R}_{\text{miss}}$ consists of numerical propagation of $\boldsymbol{R}$ and $\boldsymbol{V}$ as a function of time using Eq. (1) or (2) and then determining the particular value of $\boldsymbol{R}$ that satisfies Eq. (3). Predictive guidance is based on this procedure.[7] For real time, onboard implementation with hit to kill performance requirements, this approach may have high computational burdens. Therefore, reliable methods of estimating $\boldsymbol{R}_{\text{miss}}$ with sufficient accuracy and convergence speed are of special interest to the guidance engineer and are addressed in the following sections.

As developed here, zero effort miss guidance attempts to null the miss distance with a conventional feedback loop. The proposed guidance law for interceptors with vectorable, continuous thrust is

$$\boldsymbol{T} = T\boldsymbol{\lambda}, \qquad \boldsymbol{\Lambda} = \varepsilon + K\boldsymbol{R}_{\text{miss}\perp} = \Lambda\boldsymbol{\lambda} \quad (4)$$

In Eq. (4), $\boldsymbol{\Lambda}$ is the commanded thrust vector orientation given by the addition of the unit vector along the line of sight $\varepsilon = \boldsymbol{R}/R$ plus the perpendicular component of the zero effort miss vector, denoted as $\boldsymbol{R}_{\text{miss}\perp}$, scaled by a guidance feedback gain K. Specifically, $\boldsymbol{R}_{\text{miss}\perp}$ is

$$\boldsymbol{R}_{\text{miss}\perp} = \boldsymbol{R}_{\text{miss}} - (\boldsymbol{R}_{\text{miss}} \cdot \varepsilon)\varepsilon \quad (5)$$

An option, which is not explored here, is to replace $\boldsymbol{R}_{\text{miss}\perp}$ with $\boldsymbol{R}_{\text{miss}}$ in Eq. (4). In this case, the component of $\boldsymbol{R}_{\text{miss}}$ along the line of sight could be collected with ε, leading back to Eq. (4).

Observe from Eq. (4) that for large miss distances the guidance law commands thrust primarily in the miss direction, whereas after the miss has been sufficiently nulled, thrust is commanded along the line of sight until burnout. For long-range targeting applications, the miss is not fully eliminated but is reduced to a steady-state value [i.e., the two terms in Eq. (4) compete for the proper thrusting direction]. The resulting effect in Eq. (4) is a stead offset from the line of slight, which corrects for the accelerations acting on the system during postburnout. A steady thrusting condition in the proper direction is conducive to both miss performance and burnout insensitivity.[14] For interceptors with on/off divert thrusting capability, ε is eliminated from Eq. (4), and thrusting is turned off when the miss distance is sufficiently nulled. Finally, note that Eq. (4) requires additional sensors for implementation, relative to a conventional intercept guidance law.

Zero Gravity

As a baseline calculation of the zero effort miss, consider the case where both vehicles experience equal acceleration, or $\boldsymbol{R}_T \approx \boldsymbol{R}_I$. In this case, Eq. (2) reduces to

$$\dot{\boldsymbol{V}} = -(1/m)\boldsymbol{T} \quad (6)$$

Integration of Eq. (6) with $\boldsymbol{T} = \boldsymbol{0}$ yields

$$\begin{aligned} \boldsymbol{V}(t) &= \boldsymbol{V}(t_i) \\ \boldsymbol{R}(t) &= \boldsymbol{V}(t_i)(t - t_i) + \boldsymbol{R}(t_i) \end{aligned} \quad (7)$$

where t_i denotes the current or initial time and t denotes some future time. Equation (7) indicates a target trajectory, relative to the interceptor, that is rectilinear.[5]

Substituting Eq. (7) into Eq. (3) and solving for t gives the final time at miss t_f or

$$t_f = t_i - \frac{\boldsymbol{R}(t_i) \cdot \boldsymbol{\rho}(t_i)}{V(t_i)} \quad (8)$$

where $\boldsymbol{\rho} = \boldsymbol{V}/V$ denotes the unit vector for $\boldsymbol{V}$. Here, a closed-form solution for t_f is possible. The zero effort miss at the current time is given by $\boldsymbol{R}(t)$ evaluated at $t = t_f$ or

$$\boldsymbol{R}_{\text{miss}}(t_i) = -\{\boldsymbol{R}(t_i) \cdot \boldsymbol{\rho}(t_i)\}\boldsymbol{\rho}(t_i) + \boldsymbol{R}(t_i) \quad (9)$$

When the vehicle separation widens, Eq. (6) and all that follows become invalid. Therefore, reconsider the full behavior in Eq. (2), rewritten as

$$\dot{\boldsymbol{V}} = \boldsymbol{G} - (1/m)\boldsymbol{T} \quad (10)$$

where

$$\begin{aligned} \boldsymbol{G} &= \boldsymbol{G}_T - \boldsymbol{G}_I \\ \boldsymbol{G}_T &= -\left(\mu/R_T^2\right)\varepsilon_T, \qquad \boldsymbol{G}_I = -\left(\mu/R_I^2\right)\varepsilon_I \end{aligned} \quad (11)$$

Since an exact closed-form expression for $\boldsymbol{G}$ in terms of $\boldsymbol{R}$, or t, is intractable and direct numerical propagation is to be avoided, the following sections consider approximations for the true behavior of $\boldsymbol{G}$.

Constant Gravity

Suppose the target position and velocity are available at the current value of time, for example, from a target state vector update or propagation from a previous update supplied by a ground- or space-based surveillance system. The current interceptor position and velocity are also available from the onboard navigation system. With this information, $\boldsymbol{G}(t_i)$ is easily determined. Also, for a near intercept, the final acceleration difference is essentially zero, or $\boldsymbol{G}(t_f) = \boldsymbol{0}$. Initially, this assumption may be in error, but as the guidance system steers the interceptor to the desired state, the validity of the assumption increases.

An average, constant model for $\boldsymbol{G}$ applicable over the zero effort trajectory is

$$\boldsymbol{G}(t) = \tfrac{1}{2}\{\boldsymbol{G}(t_f) + \boldsymbol{G}(t_i)\} = \boldsymbol{C}_0(t_i) \quad (12)$$

Realize that during each miss calculation, $\boldsymbol{G}$ is held constant; however, each time a guidance solution is computed, $\boldsymbol{C}_0$ is updated reflecting the new geometry. Integration of Eq. (10) ($\boldsymbol{T} = \boldsymbol{0}$) with the gravity model in Eq. (12) gives

$$\begin{aligned} \boldsymbol{V}(t) &= \boldsymbol{C}_0(t_i)(t - t_i) + \boldsymbol{V}(t_i) \\ \boldsymbol{R}(t) &= \tfrac{1}{2}\boldsymbol{C}_0(t_i)(t - t_i)^2 + \boldsymbol{V}(t_i)(t - t_i) + \boldsymbol{R}(t_i) \end{aligned} \quad (13)$$

Observe from Eq. (13) that the constant acceleration model leads to curvature (second-order polynomial) in the target trajectory, relative to the interceptor.

Substituting Eq. (13) into Eq. (3), letting $t = t_f$, and dropping the functional dependence notation yield the following cubic equation for the time at miss:

$$\begin{aligned} &\left\{\tfrac{1}{2}\boldsymbol{C}_0 \cdot \boldsymbol{C}_0\right\}(t_f - t_i)^3 + \left\{\tfrac{3}{2}\boldsymbol{C}_0 \cdot \boldsymbol{V}\right\}(t_f - t_i)^2 \\ &\quad + \left\{\boldsymbol{C}_0 \cdot \boldsymbol{R} + \boldsymbol{V} \cdot \boldsymbol{V}\right\}(t_f - t_i) + \{\boldsymbol{V} \cdot \boldsymbol{R}\} = 0 \end{aligned} \quad (14)$$

Here, the solution for the intercept time involves finding the roots of a polynomial. Finally, substitution of the intercept time back into Eq. (13) determines the zero effort miss:

$$\boldsymbol{R}_{\text{miss}}(t_i) = \tfrac{1}{2}\boldsymbol{C}_0(t_i)(t_f - t_i)^2 + \boldsymbol{V}(t_i)(t_f - t_i) + \boldsymbol{R}(t_i) \quad (15)$$

As before, this serves as input to the guidance law in Eq. (4).

It can be seen from Eqs. (13–15) that if C_0 is set to zero, the baseline estimation of the miss given by Eqs. (7–9) results. On the other hand, notice how C_0 introduces new higher order terms in the governing relationships. The intent here is to more accurately approximate the true inverse square behavior, as compared with the baseline calculation, thereby leading to higher accuracy in the R_{miss} calculation.

Linear Gravity

Consider a linear model for G or

$$G(t) = \frac{G(t_i)}{(t_f - t_i)}(t_f - t) = C_1(t_i, t_f)(t_f - t) \tag{16}$$

From Eq. (16) observe that for $t = t_i$ the model gives $G(t_i)$, for $t = t_f$ the model gives $\mathbf{0}$, and in between linear interpolation occurs. Integration of Eq. (10) using the linear model for G in Eq. (16) and with $T = \mathbf{0}$ yields

$$\begin{aligned} V(t) &= \tfrac{1}{2}C_1(t_i, t_f)\left\{(t_f - t_i)^2 - (t_f - t)^2\right\} + V(t_i) \\ R(t) &= \tfrac{1}{2}C_1(t_i, t_f)\left\{\tfrac{1}{3}\left[(t_f - t)^3 - (t_f - t_i)^3\right]\right. \\ &\quad \left. + (t_f - t_i)^2(t - t_i)\right\} + V(t_i)(t - t_i) + R(t_i) \end{aligned} \tag{17}$$

Here, the relative motion is governed by a third-order polynomial trajectory.

Substituting Eq. (17) into Eq. (3) with $t = t_f$ and dropping the functional dependence notation yields a cubic equation for the time at miss [recall that $(t_f - t_i)$ appears in the denominator of $C_1(t_i, t_f)$],

$$\begin{aligned} &\left\{\tfrac{1}{6}C_1 \cdot C_1\right\}(t_f - t_i)^5 + \left\{\tfrac{5}{6}C_1 \cdot V\right\}(t_f - t_i)^3 \\ &\quad + \left\{\tfrac{1}{2}C_1 \cdot R\right\}(t_f - t_i)^2 + \{V \cdot V\}(t_f - t_i) + \{V \cdot R\} = 0 \end{aligned} \tag{18}$$

and a zero effort miss of

$$R_{\text{miss}}(t_i) = \tfrac{1}{3}C_1(t_i, t_f)(t_f - t_i)^3 + V(t_i)(t_f - t_i) + R(t_i) \tag{19}$$

Quadratic Gravity

Now focus attention on a quadratic model for G. Suppose that, in addition to having the current value of G, another value is available at some previous time t_p $(t_p < t_i)$, i.e., $G(t_p)$. This represents a past value that is stored in the flight computer, possibly describing the geometry at the initial update of the target state vector, supplied to the interceptor before midcourse guidance commences.

A quadratic model for the G behavior is then

$$G(t) = C_2(t_p, t_i, t_f)(t_f - t)^2 + C_1(t_p, t_i, t_f)(t_f - t) \tag{20}$$

To determine the constants C_1 and C_2, consider evaluating Eq. (20) at times t_p and t_i or

$$\begin{bmatrix} (t_f - t_p)(t_f - t_p)^2 \\ (t_f - t_i)(t_f - t_i)^2 \end{bmatrix} \begin{bmatrix} C_1(t_p, t_i, t_f) \\ C_2(t_p, t_i, t_f) \end{bmatrix} = \begin{bmatrix} G(t_p) \\ G(t_i) \end{bmatrix} \tag{21}$$

Inverting the linear matrix Eq. (21) gives C_1 and C_2 or

$$\begin{aligned} C_1(t_p, t_i, t_f) &= -\frac{G(t_p)(t_f - t_i)}{(t_f - t_p)(t_i - t_p)} + \frac{G(t_i)(t_f - t_p)}{(t_f - t_i)(t_i - t_p)} \\ C_2(t_p, t_i, t_f) &= \frac{G(t_p)}{(t_f - t_p)(t_i - t_p)} - \frac{G(t_i)}{(t_f - t_i)(t_i - t_p)} \end{aligned} \tag{22}$$

Observe from Eqs. (20) and (22) that for $t = t_p$ the model gives $G(t_p)$, for $t = t_i$ the model gives $G(t_i)$, for $t = t_f$ the model gives $\mathbf{0}$, and in between quadratic interpolation occurs.

Integration of Eq. (10) with Eq. (20) gives

$$\begin{aligned} V(t) &= \tfrac{1}{3}C_2(t_p, t_i, t_f)\left\{(t_f - t_i)^3 - (t_f - t)^3\right\} \\ &\quad + \tfrac{1}{2}C_1(t_p, t_i, t_f)\left\{(t_f - t_i)^2 - (t_f - t)^2\right\} + V(t_i) \\ R(t) &= \tfrac{1}{3}C_2(t_p, t_i, t_f)\left\{\tfrac{1}{4}\left[(t_f - t)^4 - (t_f - t_i)^4\right]\right. \\ &\quad \left. + (t_f - t_i)^3(t - t_i)\right\} + \tfrac{1}{2}C_1(t_p, t_i, t_f)\left\{\tfrac{1}{3}\left[(t_f - t)^3\right.\right. \\ &\quad \left.\left. - (t_f - t_i)^3\right] + (t_f - t_i)^2(t - t_i)\right\} + V(t_i)(t - t_i) + R(t_i) \end{aligned} \tag{23}$$

Note that a quadratic model for G has upped the relative trajectory to a fourth-order polynomial.

Substituting Eq. (23) into Eq. (3) with $t = t_f$ and dropping the functional dependence notation yields

$$\begin{aligned} &\left\{\tfrac{1}{12}C_2 \cdot C_2\right\}(t_f - t_i)^7 + \left\{\tfrac{17}{72}C_2 \cdot C_1\right\}(t_f - t_i)^6 \\ &\quad + \left\{\tfrac{1}{6}C_1 \cdot C_1\right\}(t_f - t_i)^5 + \left\{\tfrac{7}{12}C_2 \cdot V\right\}(t_f - t_i)^4 \\ &\quad + \left\{\tfrac{1}{3}C_2 \cdot R + \tfrac{5}{6}C_1 \cdot V\right\}(t_f - t_i)^3 \\ &\quad + \left\{\tfrac{1}{3}C_2 \cdot R + \tfrac{5}{6}C_1 \cdot V\right\}(t_f - t_i)^3 + \{V \cdot R\} = 0 \end{aligned} \tag{24}$$

This is a seventh-order equation for t_f after $(t_f - t_p)$ and $(t_f - t_i)$ are cleared from the denominators of C_1 and C_2. Finally, the zero effort miss becomes

$$\begin{aligned} R_{\text{miss}}(t_i) &= \tfrac{1}{4}C_2(t_p, t_i, t_f)(t_f - t_i)^4 + \tfrac{1}{3}C_1(t_p, t_i, t_f)(t_f - t_i)^3 \\ &\quad + V(t_i)(t_f - t_i) + R(t_i) \end{aligned} \tag{25}$$

Linearized Inverse Square Gravity

In the preceding sections, the approximations for G might be categorized as the mathematical approach. Here, a spaceflight mechanics-based approach is considered. Recall the original governing relationship in Eq. (2). Eliminating the target position from Eq. (2) with $R_T = R_I + R$ and the law of cosines or

$$R_T^2 = R_I^2 + R^2 + 2(R \cdot R_I) \tag{26}$$

yields

$$\dot{V} = -\frac{\mu}{R_I^2}\left\{\frac{\varepsilon_I + (R/R_I)\varepsilon}{\left[1 + (R/R_I)^2 + 2(R/R_I)(\varepsilon \cdot \varepsilon_I)\right]^{\frac{3}{2}}} - \varepsilon_I\right\} - \frac{1}{m}T \tag{27}$$

Using the binomial expansion, Eq. (27) becomes

$$\dot{V} = -\left(\mu/R_I^2\right)(R/R_I)\{\varepsilon - 3[\varepsilon \cdot \varepsilon_I]\varepsilon_I + \cdots\} - (1/m)T \tag{28}$$

If the relative position is small compared with the interceptor position $(R \ll R_I)$, then the higher order terms become small and are neglected, leading to the classic Clohessy–Wiltshire equations governing the relative motion[15,16]:

$$\dot{V} = -\left(\mu/R_I^2\right)(R/R_I)\{\varepsilon - 3[\varepsilon \cdot \varepsilon_I]\varepsilon_I\} - (1/m)T \tag{29}$$

With $T = \mathbf{0}$, Eq. (29) is a vector, homogeneous, linear, second-order, ordinary differential equation in R with time-varying coefficients. If the engagement geometry is restricted to the case where the interceptor position vector remains roughly constant (i.e., $R_I(t) = R_{Ic}$), then Eq. (29) becomes time invariant and closed-form solutions are possible. Because of the inherent assumptions listed earlier, Eq. (29) is invalid for extremely long targeting ranges or when large interceptor positional changes occur. However, these situations are not encountered in the midcourse phase as presented in this work.

With R_{Ic}, R, and V expressed in component form as

$$\begin{aligned} R_{Ic} &= X_{Ic}i + Y_{Ic}j + Z_{Ic}k \\ R &= Xi + Yj + Zk \\ V &= \dot{X}i + \dot{Y}j + \dot{Z}k \end{aligned} \tag{30}$$

the physical vector Eq. (29) can be rewritten as the following algebraic vector equation ($T = \mathbf{0}$):

$$\begin{aligned} &\ddot{\bar{R}} + \bar{\Omega}\bar{R} = \bar{0}, \qquad \bar{R} = [XYZ]^T \\ &\bar{\Omega} = \frac{\mu}{R_{Ic}^3}\left\{\bar{I} - 3\bar{R}_{Ic}\bar{R}_{Ic}^T/R_{Ic}^2\right\}, \qquad \bar{R}_{Ic} = [X_{Ic}Y_{Ic}Z_{Ic}]^T \end{aligned} \tag{31}$$

In state space form, Eq. (31) becomes

$$\underbrace{\begin{bmatrix}\dot{\bar{R}}\\ \ddot{\bar{R}}\end{bmatrix}}_{\dot{\bar{X}}} = \underbrace{\begin{bmatrix}\bar{0} & \bar{I}\\ -\bar{\Omega} & \bar{0}\end{bmatrix}}_{\bar{A}} \underbrace{\begin{bmatrix}\bar{R}\\ \dot{\bar{R}}\end{bmatrix}}_{\bar{X}} \tag{32}$$

Observe that the state dynamics matrix $\bar{A}$ is solely a function of the interceptor position.

The solution to Eq. (32) can be written as

$$\bar{X}(t) = e^{\bar{A}(t-t_i)}\bar{X}(t_i) \tag{33}$$

with

$$e^{\bar{A}(t-t_i)} = \bar{I} + \bar{A}(t-t_i) + \tfrac{1}{2}\bar{A}^2(t-t_i)^2 + \tfrac{1}{6}\bar{A}^3(t-t_i)^3 + \tfrac{1}{24}\bar{A}^4(t-t_i)^4 + \cdots \tag{34}$$

From Eq. (33), $\dot{\bar{R}}(t)$ and $\bar{R}(t)$ are thus

$$\dot{\bar{R}}(t) = \left\{\bar{I} - \tfrac{1}{2}\bar{\Omega}(t-t_i)^2 + \tfrac{1}{24}\bar{\Omega}^2(t-t_i)^4 + \cdots\right\}\dot{\bar{R}}(t_i) + \left\{-\bar{\Omega}(t-t_i) + \tfrac{1}{6}\bar{\Omega}^2(t-t_i)^3 + \cdots\right\}\bar{R}(t_i) \tag{35}$$

$$\bar{R}(t) = \left\{\bar{I}(t-t_i) - \tfrac{1}{6}\bar{\Omega}(t-t_i)^3 + \cdots\right\}\dot{\bar{R}}(t_i) + \left\{\bar{I} - \tfrac{1}{2}\bar{\Omega}(t-t_i)^2 + \tfrac{1}{24}\bar{\Omega}^2(t-t_i)^4 + \cdots\right\}\bar{R}(t_i)$$

Observe from Eq. (35) that the linearized inverse square model is a generalization of the previous models in the sense that the relative trajectory is now governed by an infinite order polynomial.

Here, Eq. (3) becomes

$$\dot{\bar{R}}^T \cdot \bar{R} = 0 \tag{36}$$

and substituting Eq. (35) into Eq. (36) with $t = t_f$ and dropping the functional dependence notation yields the equation for the time at miss or

$$\cdots + \left\{\tfrac{2}{3}\dot{\bar{R}}^T\bar{\Omega}^2\bar{R}\right\}(t-t_i)^4 + \left\{-\tfrac{2}{3}\dot{\bar{R}}^T\bar{\Omega}\dot{\bar{R}} + \tfrac{2}{3}\bar{R}^T\bar{\Omega}^2\bar{R}\right\}(t-t_i)^3 + \{-2\dot{\bar{R}}^T\bar{\Omega}\bar{R}\}(t-t_i)^2 + \{\dot{\bar{R}}^T\dot{\bar{R}} - \bar{R}^T\bar{\Omega}\bar{R}\}(t-t_i) + \{\dot{\bar{R}}^T\bar{R}\} = 0 \tag{37}$$

Equation (37) is also an infinite order polynomial. Finally, substitution of the time at miss back into $\bar{R}$ in Eq. (35) yields the zero effort miss, which is input to the guidance law in Eq. (4):

$$\bar{R}_{\text{miss}}(t_i) = \left\{\bar{I}(t_f - t_i) - \tfrac{1}{6}\bar{\Omega}(t_f - t_i)^3 + \cdots\right\}\dot{\bar{R}}(t_i) + \left\{\bar{I} - \tfrac{1}{2}\bar{\Omega}(t_f - t_i)^2 + \tfrac{1}{24}\bar{\Omega}^2(t_f - t_i)^4 + \cdots\right\}\bar{R}(t_i) \tag{38}$$

In this formulation, an appropriate value for $\boldsymbol{R}_{Ic}$ must be selected that is applicable over the interceptor trajectory. The simplest choice is to use the current value of $\boldsymbol{R}_I$ or

$$\boldsymbol{R}_{Ic} = \boldsymbol{R}_I(t_i) \tag{39}$$

Another choice is an average value between the current $\boldsymbol{R}_I$ and $(\boldsymbol{R}_I + \frac{1}{2}\boldsymbol{R})$:

$$\boldsymbol{R}_{Ic} = \tfrac{1}{2}\left[\boldsymbol{R}_I(t_i) + \left\{\boldsymbol{R}_I(t_i) + \tfrac{1}{2}\boldsymbol{R}(t_i)\right\}\right] = \boldsymbol{R}_I(t_i) + \tfrac{1}{4}\boldsymbol{R}(t_i) \tag{40}$$

This value assumes the intercept will take place at the midpoint of $\boldsymbol{R}$. A final choice for $\boldsymbol{R}_{Ic}$ is a more realistic average using the interceptor velocity to estimate where the collision takes place along $\boldsymbol{R}$. This value is given by

$$\boldsymbol{R}_{Ic} = \tfrac{1}{2}[\boldsymbol{R}_I(t_i) + \{\boldsymbol{R}_I(t_i) + [\boldsymbol{V}_I(t_i)\cdot\varepsilon(t_i)]\varepsilon(t_i)(\tilde{t}_f - t_i)\}] \tag{41}$$

$$\tilde{t}_f = t_i - \frac{R(t_i)}{\boldsymbol{V}(t_i)\cdot\varepsilon(t_i)}$$

Although $\boldsymbol{R}_I$ is assumed constant during the coast along the zero effort trajectory, note $\boldsymbol{R}_{Ic}$ can be updated at each guidance solution to reflect the changing geometry.

Example

The merits and/or deficiencies of the guidance strategies in the previous sections are investigated next in a satellite intercept scenario. The target is in a 500-km-altitude circular orbit that corresponds to a velocity of 7.6 km/s. The interceptor states at midcourse burn ignition are a velocity of 3 km/s, flight-path angle of 70 deg, and altitude of 100 km. Further, ignition occurs 168 s before the target is directly overhead of the interceptor position at ignition. For the quadratic approximation, t_p is taken 5 s before ignition. Also, the initial relative position and velocity magnitudes are 1303 km and 8.6 km/s, whereas the angle between $\boldsymbol{R}$ and $-\boldsymbol{V}$ is 3.1 deg. Midcourse burn lasts 15 s via a solid propellant system with no cutoff capability. Interceptor mass and thrust are 300 kg and 4(250 kg)(9.81 m/s^2). Propellant contributes 250 kg to the 300-kg total. All simulations are run with a guidance gain of 0.0004 1/m.

The overall guidance performance results from two major contributions: 1) the effectiveness of the guidance feedback loop in controlling the predicted miss and 2) the fidelity of the predicted miss. These two contributions are apparent in Figs. 2–6. In these figures, for time between ignition and burnout, the corresponding miss at the end of the zero effort trajectory is shown. Actually, for each time, two flyouts are conducted using 1) direct numerical propagation (true) and 2) approximate gravity solution (predicted).

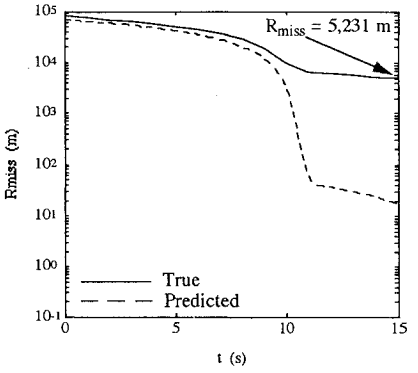

Fig. 2 Guidance performance using zero gravity.

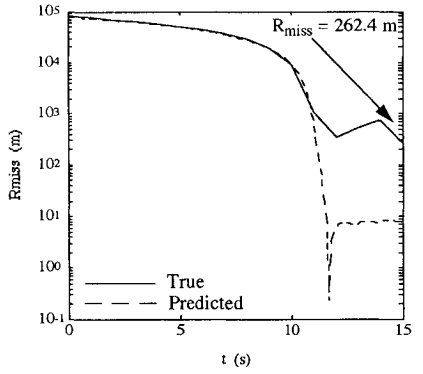

Fig. 3 Guidance performance using constant gravity.

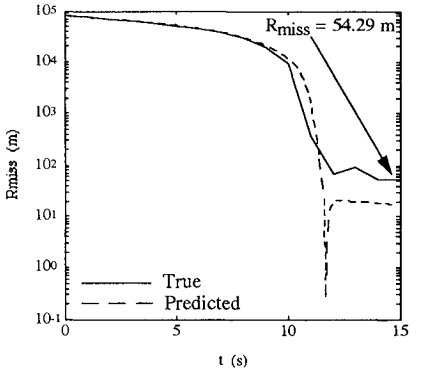

Fig. 4 Guidance performance using linear gravity.

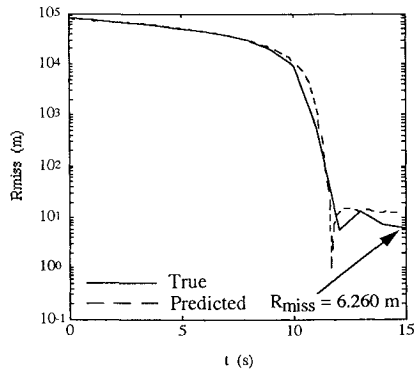

Fig. 5 Guidance performance using quadratic gravity.

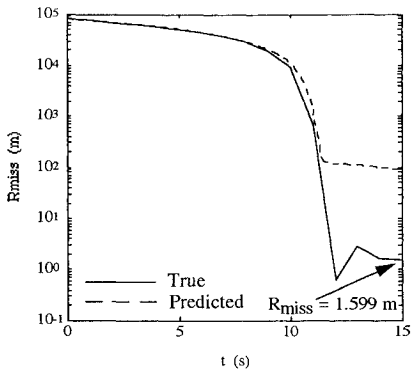

Fig. 6 Guidance performance using linearized inverse square gravity.

Recall that the true miss at burnout, which is highlighted in each figure, corresponds to the actual minimum value of $\boldsymbol{R}$ as the target swings by the interceptor.

In Figs. 2–6, the effectiveness of the guidance loop is clearly indicated. The large initial predicted miss is significantly reduced after 11 to 12 s. Observe in the figures how the predicted miss is driven to a critical value with little improvement afterwards. The guidance law has converged to a steady-state thrusting direction that corrects for the postburnout accelerations as best it can. With the abscissa representing miss magnitude, the sharp dips in the traces correspond to overshoot. The rapid convergence to a steady-state condition demonstrated here is not attainable if attitude dynamics, software rate limiting, and control system time delays are accounted for. However, the results demonstrate the ultimate potential of the guidance law in Eq. (4).

The fidelity of the predicted miss is also indicated in Figs. 2–6 by the difference between the true and predicted curves. The baseline case (zero gravity) is clearly inadequate for orbital intercepts at this targeting range (if the interceptor endgame divert capability is on the order of 5000 m or less). Note the closed-loop limit cycling in the true miss curves due to the digital nature of the simulation. As the sophistication in estimating the miss increases from constant to quadratic approximations, an improving trend in the miss prediction fidelity is noted. At burnout, the true misses range from 262.4 m for the constant approximation to 6.260 m for the quadratic approximation. The fidelity indicated here will degrade, of course, as corrupted measurements for the vehicle state vectors are considered, or targeting range increases.

As noted previously, higher performance is expected from the linearized inverse square technique because of the infinite order polynomial generalization. Figure 6 confirms this expectation showing a miss of 1.599 m for the technique. In generating Fig. 6, the infinite order polynomials were truncated to fourth order, and Eq. (40) was used for $\boldsymbol{R}_{Ic}$. The origins of this improved performance can be traced back to a key feature in the Eq. (29) gravity model, as discussed next.

Observe from Eq. (11) that if $\boldsymbol{R}_I \parallel \boldsymbol{R}_T$ (colinear position vectors), then the orientation of $\boldsymbol{G}$ lies along $\boldsymbol{R}$, and the magnitude of $\boldsymbol{G}$ is driven by the altitude difference. On the other hand, if $R_T \approx R_I$ (equal altitudes), note that the orientation of $\boldsymbol{G}$ is again parallel to $\boldsymbol{R}$, but the magnitude of $\boldsymbol{G}$ is driven by the directional cosine angle between the position vectors. In the general case where both altitude differences and directional cosine angles vary, $\boldsymbol{G}$ is not necessarily aligned with $\boldsymbol{R}$. However, the components of $\boldsymbol{G}$ tend to rotate with $\boldsymbol{R}$, and the normal component goes to zero for the special cases noted earlier.

For the constant and linear approximations in Eqs. (12) and (16), note that $\boldsymbol{G}(t)$ is anchored to the initial direction $\boldsymbol{G}(t_i)$. The same restriction holds for the quadratic approximation in Eq. (20) with t_i and t_p separated by only 5 s. Therefore, during the zero effort flyout prediction, $\boldsymbol{G}$ does not rotate with $\boldsymbol{R}$ and key acceleration information normal to $\boldsymbol{G}(t_i)$ is missing. These gravity approximations capture the magnitude variations but not necessarily the orientation changes. In contrast, for the spaceflight-based gravity approximation in Eq. (29), $\boldsymbol{G}$ is an explicit function of $\boldsymbol{R}$ and is allowed to track the line of sight during the zero effort flyout. Additionally, the two gravitational terms on the right-hand side of Eq. (29) capture the characteristics of $\boldsymbol{G}$ noted in the previous paragraph. This extra freedom in the gravity approximation allows for superior guidance performance.

Guidance Gain Selection

As a first cut at selecting the guidance gain in Eq. (4), consider a formal linearization of the guidance law and the zero gravity approximation. With respect to Fig. 1, construct a line of sight frame with unit vectors $\boldsymbol{\varepsilon}$ along $\boldsymbol{R}$ and $\boldsymbol{n}$ normal to $\boldsymbol{R}$ lying in the $\boldsymbol{R} - \boldsymbol{V}$ plane oriented to the $\boldsymbol{V}$ side of $\boldsymbol{R}$. Introduce components for the relevant vectors or

$$
\begin{aligned}
\boldsymbol{R} &= R\boldsymbol{\varepsilon} \\
\boldsymbol{V} &= \dot{R}\boldsymbol{\varepsilon} + V_n\boldsymbol{n} = V_\varepsilon\boldsymbol{\varepsilon} + V_n\boldsymbol{n} \\
\dot{\boldsymbol{V}} &= \left[\dot{V}_\varepsilon - \left(V_n^2/R\right)\right]\boldsymbol{\varepsilon} + \left[\dot{V}_n + \left(V_nV_\varepsilon/R\right)\right]\boldsymbol{n} \\
\boldsymbol{R}_{\text{miss}} &= R_{\text{miss}\,\varepsilon}\boldsymbol{\varepsilon} + R_{\text{miss}\,n}\boldsymbol{n} \\
\boldsymbol{R}_{\text{miss}\perp} &= R_{\text{miss}\perp n}\boldsymbol{n} \\
\boldsymbol{T} &= T_\varepsilon\boldsymbol{\varepsilon} + T_n\boldsymbol{n}
\end{aligned}
\tag{42}
$$

In scalar form, Eqs. (4–6) and (9) are

$$
\begin{gathered}
\dot{R} = V_\varepsilon \\
\dot{V}_\varepsilon - \left(V_n^2/R\right) = -(1/m)T_\varepsilon \qquad \dot{V}_n + \left(V_nV_\varepsilon/R\right) = -(1/m)T_n \\
R_{\text{miss}\,\varepsilon} = R\left(1 - \frac{V_\varepsilon^2}{V_\varepsilon^2 + V_n^2}\right) \qquad R_{\text{miss}\,n} = -R\frac{V_\varepsilon V_n}{V_\varepsilon^2 + V_n^2} \\
R_{\text{miss}\perp n} = R_{\text{miss}\,n} \\
T_\varepsilon = T\frac{1}{\left[1 + K^2R_{\text{miss}\perp n}^2\right]^{\frac{1}{2}}} \qquad T_n = T\frac{KR_{\text{miss}\perp n}}{\left[1 + K^2R_{\text{miss}\perp n}^2\right]^{\frac{1}{2}}}
\end{gathered}
\tag{43}
$$

Figure 7 is the time domain block diagram for this closed-loop system.

Obviously, the $V_n - T_n$ channel is the key to reducing the miss. Therefore, to simplify matters, consider a fixed R and V_ε and focus

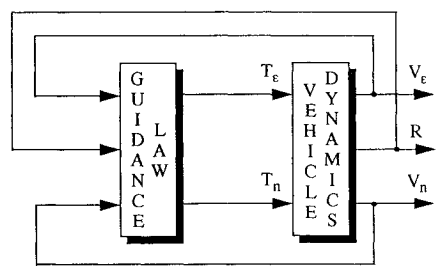

Fig. 7 Closed-loop guidance system.

attention on this loop. The vehicle dynamics and guidance law are thus

$$\dot{V}_n + (V_n V_\varepsilon / R) = -(1/m)T_n$$
$$T_n = -T \frac{K R V_\varepsilon V_n}{\left[\left(V_\varepsilon^2 + V_n^2\right)^2 + K^2 R^2 V_\varepsilon^2 V_n^2\right]^{\frac{1}{2}}} \tag{44}$$

Here, the vehicle dynamics are linear, but the guidance law still requires linearization, an easy task left to the reader. In this linear framework, a preliminary gain can be selected using conventional frequency domain techniques. Of course, extensive nonlinear simulation is required to validate and/or to tune the gain. This analytical framework can also assist in scheduling the gain due to variations in the range (R), closing velocity ($-V_\varepsilon$), and thrust (T).

Other key features are apparent from this analysis. Observe from Eq. (44) that the guidance gain does not enter into the dynamics as a pure "loop" gain but rather appears in both the numerator and denominator of T_n. For a large value of $\boldsymbol{R}_{\text{miss}\perp}(|\boldsymbol{R}_{\text{miss}\perp}| \gg 1/K)$, observe how the guidance gain is washed out. In contrast, for smaller values of $\boldsymbol{R}_{\text{miss}\perp}(|\boldsymbol{R}_{\text{miss}\perp}| \ll 1/K)$, the guidance gain behaves as a pure "loop" gain. Also, as the range approaches zero, note the guidance law avoids infinite acceleration commands.

Comparison with Augmented Proportional Navigation

In concept, the proposed guidance policy is similar to augmented proportional navigation (APN). Additional terms are included in the miss calculation to correct for accelerations. However, significant differences also exist between the techniques. Here, corrections are made for gravitational accelerations, whereas APN corrects for target accelerations. In Refs. 6 and 7, APN only considers constant accelerations normal to the line of sight. Further, the derivation is conducted with a simplified model for the miss that considers only the normal component. In this work, variable accelerations along and normal to the line of sight are addressed. Further, the derivation makes use of the full model for the miss. If the target accelerations are known, then modification of the proposed technique to account for target maneuvers appears straightforward.

Conclusions

Zero effort miss guidance, when corrected for the differential gravity effect, appears to have potentially wider applicability to strategic intercepts than just during the close range, endgame phase. The guidance law itself has been shown to be quiet effective in controlling the predicted zero effort miss, whereas the more refined miss prediction techniques provide a close match to the true miss, at least for targeting ranges out to roughly 1000 km. A clear trend of improving fidelity in the various miss prediction techniques is observed in the results, with a tradeoff of increased sophistication. Of the approximations considered for the true differential gravity effect based on accuracy alone and under all of the modeling assumptions, the linearized inverse square approximation appears superior with the quadratic and linear models not far behind. Variable direction for the gravity acceleration vector during zero effort flyouts is the key feature imbedded into the linearized inverse square approximation, which the other techniques lack. Note that any determination of the suitability of the proposed guidance law for a specific application must also consider the endgame divert capability of the interceptor.

Acknowledgments

This work was partially performed under Strategic Defense Initiative Organization Contract SDIO84-90-C-0004. Thanks go out to Dean Zes and the Guidance and Control Group, Orbital Sciences Corporation Chandler, Arizona.

References

[1]Scott, W. B., "LEAP Begins Flight Tests to Demonstrate Kinetic Kill Missile Defense Capability," *Aviation Week and Space Technology*, Vol. 134, No. 24, 1991, p. 207.

[2]Locke, A. S., et al., *Principles of Guided Missile Design*, D. Van Nostrand Co., Princeton, NJ, 1955.

[3]Adler, F. P., "Missile Guidance by Three-Dimensional Proportional Navigation," *Journal of Applied Physics*, Vol. 27, No. 5, 1956, pp. 500–507.

[4]Murtaugh, S. A., and Criel, H. E., "Fundamentals of Proportional Navigation," *IEEE Spectrum*, Vol. 3, No. 12, 1966, pp. 75–85.

[5]Abzug, M. J., "Vector Methods in Homing Guidance," *Journal of Guidance and Control*, Vol. 2, No. 3, 1979, pp. 253–255.

[6]Nesline, F. W., and Zarchan, P., "A New Look at Classical vs Modern Homing Missile Guidance," *Journal of Guidance and Control*, Vol. 4, No. 1, 1981, pp. 78–85.

[7]Zarchan, P., *Tactical and Strategic Missile Guidance*, edited by P. Zarchan, Vol. 124, Progress in Astronautics and Aeronautics, AIAA, Washington, DC, 1990.

[8]Chatterji, G. B., and Pachter, M., "A Midcourse Estimation and Guidance Law for Space Based Interceptors," *Proceedings of the American Control Conference* (San Diego, CA), American Automatic Control Council, Green Valley, AZ, 1990, pp. 2858–2862.

[9]Zes, D., "Exo-Atmospheric Intercept Using Modified Proportional Guidance with Gravity Correction for Coast Phase," AIAA Paper 94-0209, Jan. 1994.

[10]Zes, D., "Exo-Atmospheric Intercept Using Lagrange's Prediction Equations," AIAA Paper 94-3750, Aug. 1994.

[11]Newman, B., "Spacecraft Intercept Guidance Using Zero Effort Miss Steering," *Proceedings of the AIAA Guidance, Navigation, and Control Conference* (Monterey, CA), AIAA, Washington DC, 1993, pp. 1707–1716.

[12]Bate, R. R., Mueller, D. D., and White, J. E., *Fundamentals of Astrodynamics*, Dover, New York, 1971.

[13]Battin, R. H., *An Introduction to the Mathematics and Methods of Astrodynamics*, edited by J. S. Przemieniecki, AIAA Education Series, AIAA, New York, 1987.

[14]Newman, B., "Robustness Evaluation of Classical vs Lambert Based Midcourse Guidance for Exoatmospheric Intercepts," *Advances in the Astronautical Sciences*, Vol. 87, *Proceedings of the AAS/AIAA Spaceflight Mechanics Meeting* (Cocoa Beach, FL), Univelt, San Diego, CA, 1994, pp. 829–841.

[15]Clohessy, W. H., and Wiltshire, R. S., "Terminal Guidance System for Satellite Rendezvous," *Journal of the Aerospace Sciences*, Vol. 27, No. 9, 1960, pp. 653–659.

[16]Mullins, L. D., "Initial Value and Two Point Boundary Value Solutions to the Clohessy–Wiltshire Equations," *Journal of the Astronautical Sciences*, Vol. 40, No. 4, 1992, pp. 487–501.